Journal of Sea Research 195 (2023) 102432

Contents lists available at ScienceDirect

Journal of Sea Research

journal homepage: www.elsevier.com/locate/seares

Assessing the impact factors and corresponding weights affecting the coastal morphology of Hsinchu Coast, Taiwan

Wei Po Huang, Jui Chan Hsu *, Chun Jhen Ye

Dept. Harbor and River Engineering, National Taiwan Ocean University, No. 2, Pei-Ning Road, Keelung 20224, Taiwan

ARTICLEINFO

Keywords:
Coastal erosion
Anthropogenic effects
Empirical orthogonal function
Morphological change

ABSTRACT

This study investigates the long-term morphological pattern of the Hsinchu coast in northwestern Taiwan using three different methods: long-term isobath and shoreline change analysis, bathymetric volume change analysis, and the empirical orthogonal function (EOF) method. Our objectives include analyzing and understanding the effects of anthropogenic structures, natural processes, and their combined impacts on coastal morphological change. The shoreline analysis and bathymetric volume analysis briefly reveal that the morphological pattern of Hsinchu coast. Then, EOF analysis is applied to identify the dominant impact factors affecting the coastal morphology near the harbor, determine the weights of the impact factors, and infer the impact range of anthropogenic structures. Moreover, the EOF analysis is divided into two-time segments—namely, the periods 2005–2010 and 2017–2021—based on different bathymetric surveys and the corresponding values of impact factors. The primary and secondary EOF modes are strongly linked to the "interaction between wave and structure" and "interaction between river discharges and structure", respectively. The spatial components of the EOF modes demonstrate that the impact range influenced by river discharges was mainly located in the northern part of the harbor, while the minimum impact range of the structures on coastal morphological interaction changes under natural factors was 3.5 km south of Hsinchu Fishing Harbor.

1. Introduction

Coastal erosion and accretion are natural phenomena that occur worldwide. However, coastal erosion is of greater concern, especially in developed countries, due to the obvious impact of coastal erosion on coastlines. Both natural processes and human activities can influence coastal morphological changes (Mentaschi et al., 2018; Komar, 1999; Gopinath and Seralathan, 2005). In Taiwan, coastal erosion is a serious issue, and the Integrated Coastal Zone Management Plan (ICZMP) of Taiwan has identified thirteen coastal hotspots suffering from severely unbalanced littoral sediment transport (Construction and Planning Agency of the Ministry of the Interior (CPAMI), 2017). This unbalance is caused by anthropogenic factors such as the construction of nearshore structures or natural factors including abnormal river discharges and extreme wave forcing. Hsinchu Fishery Harbor, located on the northwestern coast of Taiwan, was constructed rapidly in the 1990s without adequate consideration and planning, resulting in a significant "groin effect" in nearby coastal areas (van Rijn, 2011). This alteration of the nearshore hydrodynamic mechanism has led to enhanced morphological changes and disruption of the littoral sediment transport balance, resulting in accumulation and erosion on the two sides of the structures, respectively (Mentaschi et al., 2018; Delgadillo-Calzadilla et al., 2014; Sumer et al., 2001; Martins and Pereira, 2014; Kim et al., 2013; Hsu et al., 2017). Numerous studies have shown that the coastal morphology around the Hsinchu coast—one of the thirteen coastal hotspots—has been modified by anthropogenic structures such as Hsinchu Fishery Harbor (Hsu et al., 2018; Huang, 2022).

It must be considered that natural factors, such as waves (Martins and Pereira, 2014), tides, currents, storms (Gopinath and Seralathan, 2005), and river discharges (Chang, 1997) also affect the coastal configuration. It should also be noted that, from 1998 to 2021, Taiwan was hit by three to four typhoons a year on average. The impact of typhoons results in not only heavy rainfall, leading to massive fluvial sediment accumulation at the estuary, but also the generation of huge waves that rapidly crash on the coastline, potentially causing severe coastal erosion. These effects of typhoons can significantly change the estuary and nearshore morphology (Holden and Marshall, 2018). The above-mentioned studies clearly demonstrated that the effects of both

* Corresponding author.
E-mail addresses: a0301@mail.ntou.edu.tw (W.P. Huang), 20652005@mail.ntou.edu.tw (J.C. Hsu), 20852006@mail.ntou.edu.tw (C.J. Ye).

https://doi.org/10.1016/j.seares.2023.102432
Received 24 May 2023; Received in revised form 4 August 2023; Accepted 7 August 2023
Available online 10 August 2023

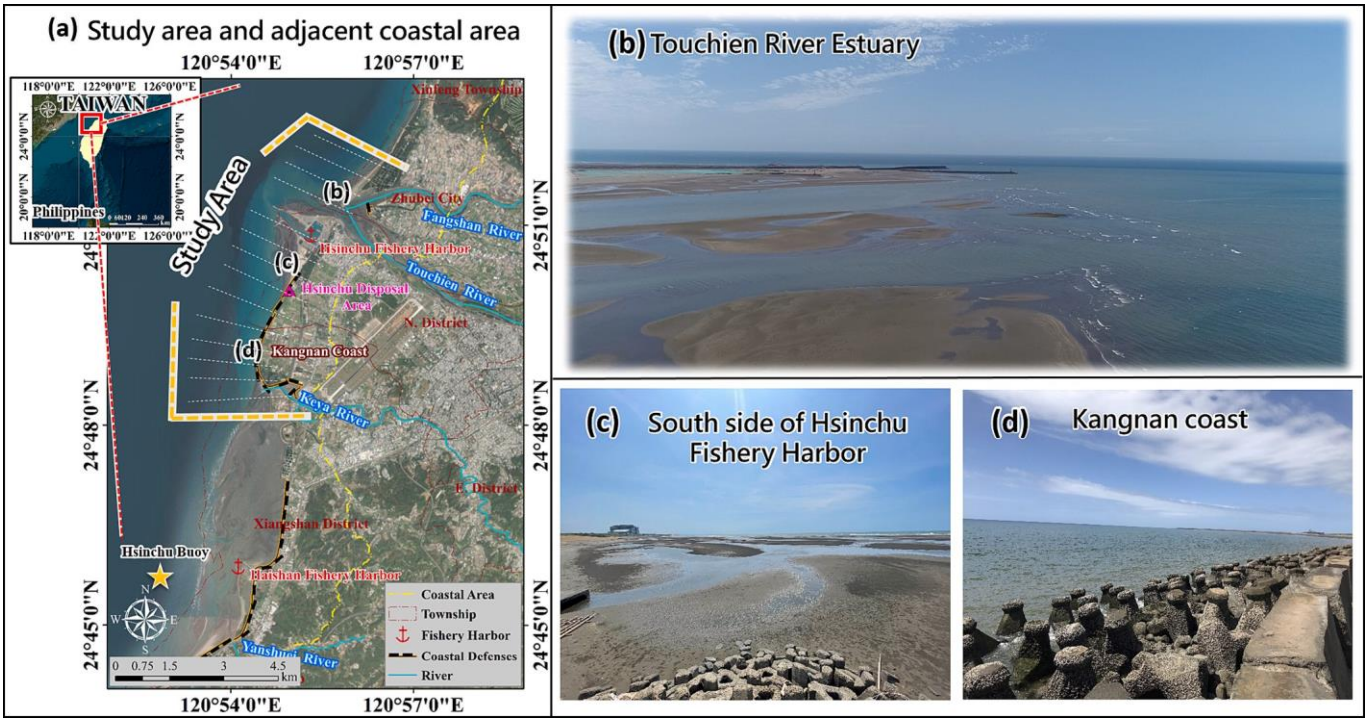

Fig. 1. (a) Detail of the study area and adjacent costal area (the yellow star represents the wave buoy, and the white dotted line represents the profiles); (b) view of Touchien River estuary; (c) view of the south of Hsinchu Fishery Harbor; (d) view of Kangnan coast of supported by Kangnan seawall. Photographs (b)–(d) taken by the authors on 17 May 2020. (For interpretation of the references to color in this figure legend, the reader is referred to the web version of this article.)

anthropogenic and natural factors play a major role in the research area—the Hsinchu coast—which has both estuaries and structures (Mentaschi et al., 2018; Komar, 1999; Gopinath and Seralathan, 2005; Nishi, 2008; Rosati, 2005, Dean, 1986, Boyd et al., 1992, Harley et al., 2015; Nicholls et al., 2007; Dalrymple et al., 2012; Masselink et al., 2016). However, in Taiwan, according to the ICZMP (Construction and Planning Agency of the Ministry of the Interior (CPAMI), 2017), it is imperative for the governing authority of Hsinchu Fishing Port to investigate the underlying causes of the abnormal sediment balance occurring in its vicinity. Subsequently, appropriate measures must be proposed to effectively mitigate this issue. Therefore, conducting a comprehensive study is crucial to examine the relationship between the impact factors and the morphological changes observed within the study area, while also determining the relative weights and ranges of influence for these factors. The obtained results would offer quantified insights for relevant government agencies and organizations, facilitating improved communication and coordination in preparation for the implementation of compensation measures.

Analysis of the coastal morphological variability provides a simple and straightfor-ward way to comprehend the rate of erosion and accretion in a coastal environment, as well as the associated evolution trend. Therefore, in recent years, analyses of coastal morphological variability, including shoreline changes, isobath changes, and sediment volume changes have been widely used in various studies considering coastal changes. These methods provide engineers with the possibility of gaining insight into the long-term, short-term, or seasonal patterns of morphological processes along a coastline (Boak and Turner, 2005). Normally, coastal morphological variability is investigated and analyzed by comparing satellite images or video images from different time periods (Gopinath and Seralathan, 2005; Tanaka et al., 2015), as well as by determining changes in volume measured through beach and bathymetric surveys in different periods (Martins and Pereira, 2014; Kim et al., 2013).

According to the ICZMP (Construction and Planning Agency of the Ministry of the Interior (CPAMI), 2017), 56.11% of the coastline around Taiwan had been covered by coastal defenses or structures, such as harbors, groins, seawalls, and revetments. When a protected shoreline suffers from severe erosion, the shoreline retreats to and is gradually controlled by the coastal defenses. Despite the fact that the historical shoreline variation would have brought about differences in the changes in the above-mentioned circumstance, it would actually have constituted a very small or negligible measurement error in this situation. This is the reason why some protected coastal regions are not easily observed when utilizing shoreline change analysis. Hence, shoreline change analysis is not a suitable method for detecting changes in some coastal regions that are protected from coastal defenses. In contrast, the use of bathymetric change analysis not only can resolve the situation where the 0 m shoreline has retreated to the structure, causing observation error but also allows more coastal morphological change information to be obtained. Although the analysis of coastal morphological variability can illustrate the coastal process at varying scales and indicate changes in coastal characteristics, the effects of impact factors cannot be quantified.

In order to verify the dominant factor influencing the nearshore morphology, this paper adopted the EOF method developed by Winant et al. (1975). EOF analysis is a data-driven method that has been employed in many studies. The EOF method not only can be used for qualitative investigation, but also provides a tool for dividing the temporal and spatial variabilities in bathymetric survey data and can identify the pattern of nearshore change (Miller and Dean, 2007a, 2007b; Taaouati et al., 2020). Many studies have used the EOF method for analysis of the coastal morphology; for example, it has been applied in the context of 1D cross-shore beach profile variation (Thanh et al., 2018; Reeve et al., 2018), 2D bathymetric surface (Buonaiuto et al., 2008; Karunarathna et al., 2008), beach nourishment (Keshtpoor et al., 2013; Habel et al., 2016), and morphological change in estuaries or riverbanks (Yuhi et al., 2013; He et al., 2019). Several recent studies have used the EOF method to determine the dominant factor affecting morphological changes (He et al., 2019; Hu et al., 2020).

This study investigates the long-term variation of isobaths and volumetric changes on the Hsinchu coast through multiple sets of field

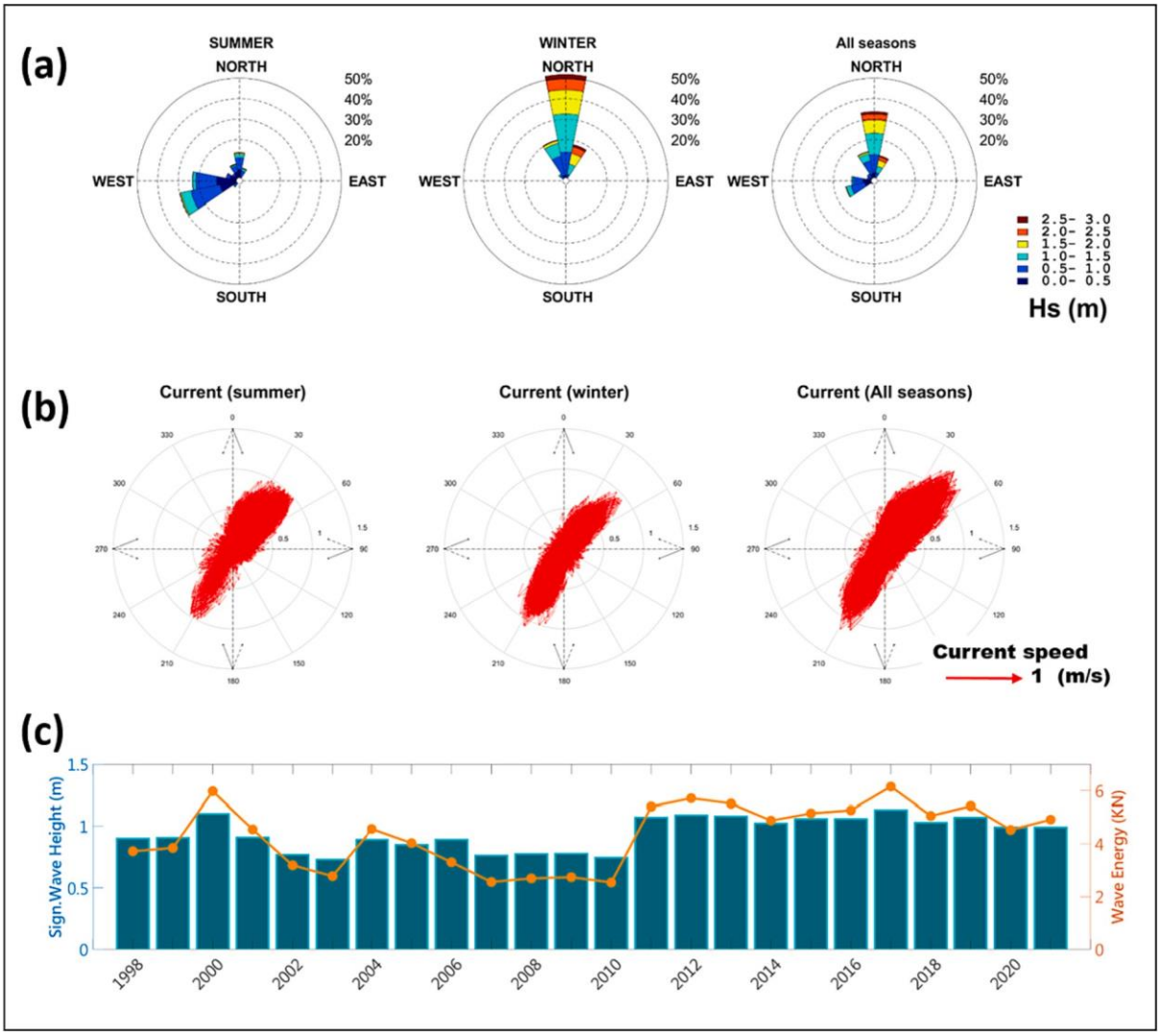

Fig. 2. (a) Directional distribution of significant wave height during summer, winter, and the time period from 1998 to 2021; (b) directional distribution of current speed during summer, winter, and the time period from 1998 to 2021; and (c) time series of yearly significant wave height (represented by green bars) and wave energy (represented by the orange line) during the time period from 1998 to 2021. (For interpretation of the references to color in this figure legend, the reader is referred to the web version of this article.)

survey data. We also examine the spatial and temporal variation of isobaths (0 m, 5 m, 10 m, 15 m, 20 m) during the pre- and post-construction periods of the Hsinchu Fishery Harbor, as well as the sediment volume variation from 1998 to 2021. Additionally, the coast is divided into three areas, based on its characteristics, and the correlations between sediment volume variation in the different areas and various impact factors are calculated. The study was conducted with the aim of identifying the dominant impact factor affecting the coastal morphology near the Hsinchu Fishery Harbor, as well as determining the weights of the impact factors and inferring the impact range of anthropogenic structures through bathymetric analyses and the EOF method. Section 1 describes the introduction, the study site, marine and fluvial information. Section 2 explains the methods used to visualize and quantify the morphological changes and interpret impact factors. Section 3 presents the results of shoreline variation, morphological changes over the past twenty years, and EOF analyses. Section 4 discusses the spatial and temporal components of the EOF results, associated with marine mechanisms, anthropogenic structures, and river discharges, as well as the impact range of the impact factors. Finally, Section 5 provides the summary and conclusions.

1.1. Description of study area

The site investigated in this paper, Hsinchu coast, is located in the northwest of Taiwan and spans 7 km from Zhubei to Kerya River. The study area is oriented NNE–SSW and includes an estuary (Touchien River estuary), an anthropogenic structure (Hsinchu Fishery Harbor), two beaches (New Moon Beach and Hsinchu Beach), and Kangnan seawall along the coast. Detailed information on the locations can be seen in Fig. 1.

Hsinchu Fishery Harbor, the most prominent anthropogenic structure in the study area, was originally built in the inner area of the estuary in 1954, in order to expand the fishery industry and to remove inefficiencies caused by the tidal harbor. Since 1981, the harbor has been rebuilt on the southern coast of the estuary to solve these problems, and it was completely finished in 1998. Hsinchu Harbor has two breakwaters: a northern one 1.1 km in length and a southern one 0.9 km in length, extending towards their respective offshore areas to secure navigation channels. The construction of a new harbor has disrupted the littoral sediment transport continuity and caused substantial changes in the coastal morphology of Hsinchu coast, mainly attributed to the presence of breakwaters (Fredsøe and Deigaard, 1992; Liou et al., 2009).

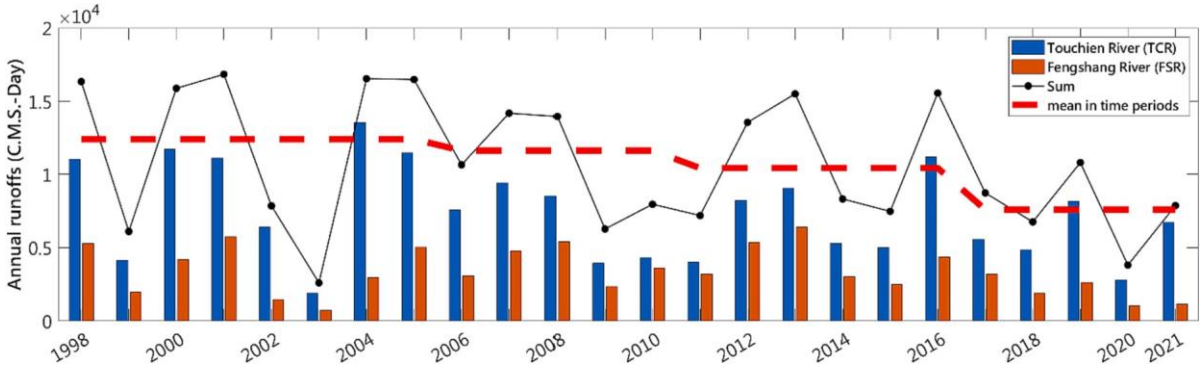

Fig. 3. Temporal variation of discharges of Touchien River (blue bar) and Fengshan River (orange bar) during the period 1998–2021. The black line represents the sum of the discharges of the two rivers, and the red dotted line represents the average river discharges in different time periods (1998–2005, 2005–2010, 2010–2017, and 2017–2021). (For interpretation of the references to color in this figure legend, the reader is referred to the web version of this article.)

As a result, anomalous erosion and accretion events have been observed around the Hsinchu Fishery Harbor over the past few decades, primarily driven by physical factors such as river discharges, marine hydraulics, and jetty effects, which occur to the north and south of the harbor (Ding and Wang, 2008).

1.2. Hydrodynamic conditions

A wave buoy is situated southwest of Hsinchu Fishery Harbor (see Fig. 1a, yellow star), 1500 m from the shore where the water depth is approximately 23 m. The wave buoy is managed and monitored by the Central Weather Bureau (CWB) of Taiwan, and it measures the details of currents and waves. Fig. 2a summarizes the wave characteristics based on hourly wave data measurements recorded by the CWB from 1992 to 2021. During the summer season (i.e., from June to August), the mean significant wave height is 0.63 m and the corresponding period is 4.3 s. The prevailing wave directions are from the west (W) and west-southwest (WSW). In contrast, in the winter season (i.e., from December to February), the influence of the strong winter monsoon results in the main wave directions being from the north (N) and north-northwest (NNW). The significant wave height is 1.3 m, and the corresponding wave period is 5.0 s. Fig. 2b depicts the dominant current directions: from north to south in winter and from south to north in summer. In this context, the littoral sediment transport is primarily affected by waves and currents, where the dominant transport directions in summer and winter are from south to north and from north to south, respectively. The wave energy during winter exceeds that of summer, resulting in the alongshore sediment transport driven by waves in the study area predominantly from north to south (Liou et al., 2009). Fig. 2c displays the mean significant wave height and wave power between 1998 and 2021. The statistical wave data show that the annual mean significant wave height has gradually increased, indicating that Hsinchu Coast has been experiencing higher wave energy year by year.

1.3. Fluvial information

Touchien River Estuary has an approximately 1.2 km wide river mouth and is fed by two rivers, Touchien River (TCR) and Fengshan River (FSR); see Fig. 1. Normally, the annual discharge of the two rivers is characterized by two periods: flood (or typhoon) season, from June to October; and a dry season, consisting of the remaining months. As can be seen from the measurements at Jeinkuo Bridge Station (station No. H017, TCR) and Hsinpu (2) Station (station No. H002, FSR), recorded by the Water Resources Agency, it is obvious that the annual discharge of TCR is higher than that of FSR, with average river discharges from 1998 to 2021 of 7334.95 m^3/s and 3347.58 m^3/s, respectively, shown in Fig. 3. Fengshan River and Touchien River merge at a common estuary located north of Hsinchu Fishery Harbor. Consequently, the discharges of both rivers are combined to establish a connection between the impact factors and the empirical orthogonal function (EOF) modes in Section 3.3.

2. Material and methods

2.1. Data sets

The coastline of the study area is approximately 8.5 km long. The bathymetric measurements for the cross-shore stretch were taken from the high tide line (HTL) to the −20 m isobath. The data used in this study were obtained from a single-beam survey with a minimum scale of 1:10,000, covering the period from 1998 to 2021. Long-term trends in shoreline and bathymetric changes were analyzed based on the bathymetric survey data. Additionally, the bathymetric survey data were used to analyze the morphological pattern through the use of the empirical orthogonal function method.

2.2. Evolution of historical isobaths and quantification of long-term morphological changes

The shoreline and isobaths (0 ~~m~~, 5 ~~m~~, 10 ~~m~~, −15 m, −20 m) from Touchien estuary to Kerya River during time periods including pre-construction (in 1983) and post-construction of Hsinchu Fishery Harbor (September 1998, September 2005, September 2010, October 2017, April 2019, and June 2021) were collected and compared to determine the evolution of historical isobaths and the spatial and temporal variation of the isobaths.

The study area has fourteen profiles (see Fig. 1a and Fig. 5), which are parallel and aligned from the north to south of Hsinchu coast, with the distance between every two profiles being 500 m. Then, the volume of erosion and accretion between two control profiles (also 13 sections) was calculated. The bathymetric survey data from different periods were compared in order to determine the sea bed changes. The accretion/erosion bathymetric volume rate (m^3/year) in different time periods was also calculated. The volumetric changes in each section were estimated from the hightide line to ~~7~~ m, which is the depth of closure (hc). Solving the inner depth of closure equation according to Hallermeier (1981), the estimated depth of closure around Hsinchu Coast is equal to 7 m (in this paper, He and Te are 3.79 m and 7.69 s, considering the statistics from Hsinchu Buoy).

2.3. EOF analysis

Furthermore, to separate the spatial and temporal components of the bathymetric survey data set and quantify the impact factors using independent modes, this paper utilized the EOF method. The EOF method is a mathematical technique used to identify a series of orthogonal

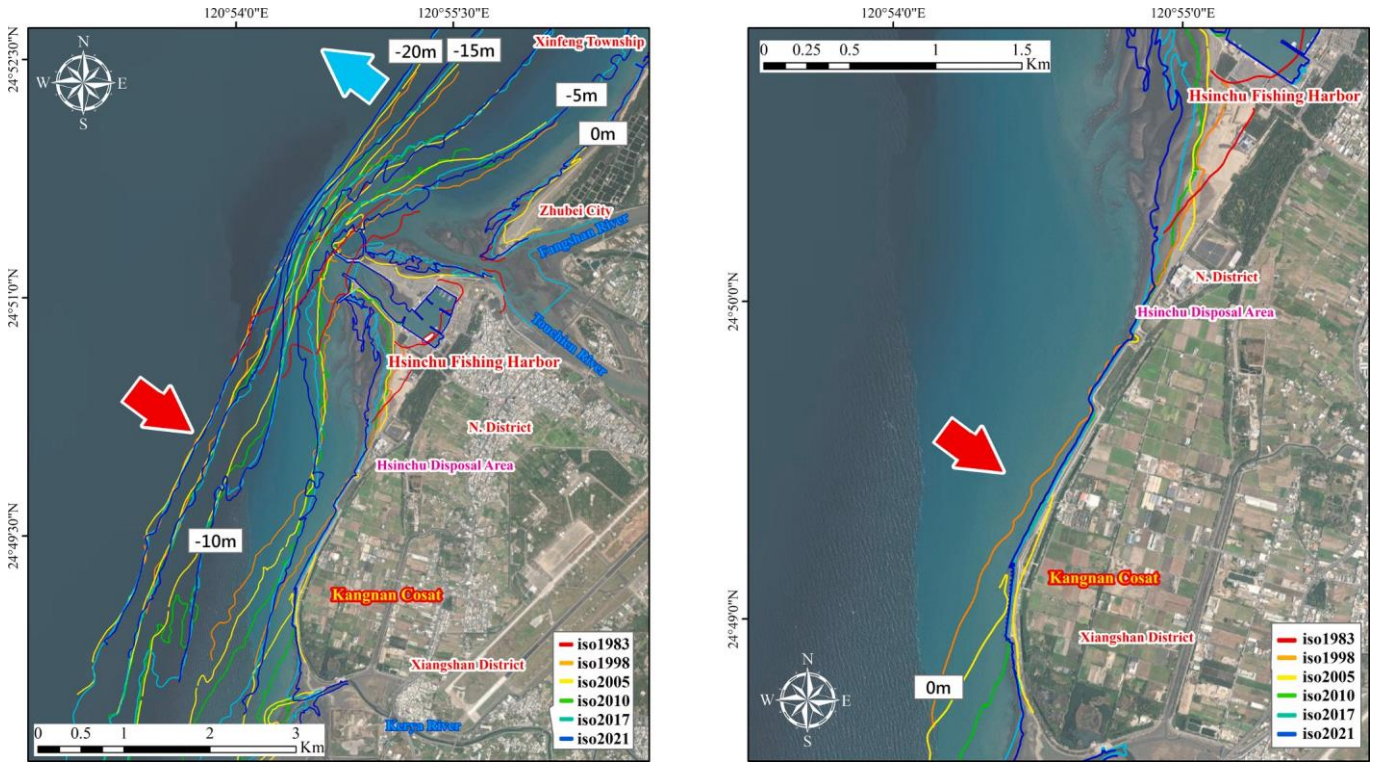

Fig. 4. Satellite images of Hsinchu Fishery Harbor and adjacent beaches: (a) The isobaths at —20 m, —15 m, —10 m, —5 m, and 0 m in different years; and (b) focus on the 0 m shoreline of Kangnan coast, on the south side of Hsinchu Fishery Harbor. The red and blue arrows represent the isobaths retreat to the land and extend to offshore, respectively. (For interpretation of the references to color in this figure legend, the reader is referred to the web version of this article.)

functions or eigenvectors, which allowed for decomposition of the original bathymetric survey data set at any given location during the study period (Alvare and Pan, 2016). The methodology utilizes spatial eigenfunctions (referred to as spatial components) and temporal eigenvectors (referred to as temporal components), —denoted as $e_n(x)$ and $c_n(t)$, respectively—which can not only be used to explain the variations in the nearshore bathymetric observed in the bathymetric surveys (Thanh et al., 2018), but enables the establishment of a link between the impact factors and the empirical orthogonal function (EOF) modes (Hu et al., 2020). The EOF method was utilized to analyze two series of bathymetric survey data: from 2005 to 2010 and from 2017 to 2021. The bathymetric surveys could thus be clearly categorized as spatial or temporal, and separated into temporal eigenvectors and spatial eigenfunctions, as detailed in Eq. (1):

$$h(x', y', t) = \sum_{n=1}^{N} c_n(t) e_n(x', y') \quad (1)$$

where h is the seabed elevation, x' and y' are the perpendicular shoreline and parallel shoreline coordinates in the latitude–longitude system, t is the year, c_n denotes the temporal eigenvectors (temporal components), e_n denotes the spatial eigenfunctions (spatial components), N is the total number of eigenfunctions, and n is the number of modes (Keshtpoor et al., 2013).

Moreover, the individual contribution rates of the impact factors can then be de-scribed using the following Eq. (2):

$$R_n = \frac{\lambda_n}{\sum_{i=1}^{N} \lambda_i} \quad (2)$$

where R_n represents the contribution rate, N is the total number of eigenfunctions, and λn is the associated eigenvalue (Thanh et al., 2018).

3. Results

3.1. Evolution of historical isobaths

Historical data on the coast, such as isobaths, shorelines, and bathymetric survey data, can provide direct insight into the long-term morphological processes and serve as key indicators for understanding the evolution of the coast. The results of this study revealed an apparent morphological change between the pre- and post-construction periods of Hsinchu Fishery Harbor, particularly in the ~~2~~0 m, ~~1~~5 m, ~~1~~0 m, ~~5~~ m, and 0 m shorelines, as shown in Fig. 4. Fig. 4a depicts the historical shorelines and isobaths in 1983 (pre-construction) and in 1998, 2005, 2010, 2017, 2019, and 2021 (post-construction). The results reveal that, after the construction of Hsinchu Fishery Harbor in 1988, the historical isobaths gradually extended to the offshore in the north of the harbor and gradually retreated to the land side in the south of the harbor, supporting the idea that the construction of Hsinchu Fishery Harbor is primarily responsible for the nearshore morphological change.

Fig. 4b focuses on Kangnan coast, presenting the historical shorelines from 1998 to 2021 after the harbor had been constructed, as well as the historical coastal lines. The shoreline retreat is significant and, after 2001, the shorelines were mostly held by the seawall. Therefore, shoreline changes alone cannot accurately capture the trend of erosion on the south side of Hsinchu Fishery Harbor.

3.2. Long-term variation of coastal morphological changes

This study selected bathymetric survey data collected in September of 1998, 2005, and 2010, as well as October 2017 and June 2021, in order to calculate the changes in bathymetric volume. The spatial pattern of coastal morphology in Hsinchu coast over the last two decades is displayed in Fig. 5, where Fig. 5a shows the bathymetric changes between 1998 and 2005, Fig. 5b shows the bathymetric changes between 2005 and 2010, Fig. 5c shows the bathymetric changes between

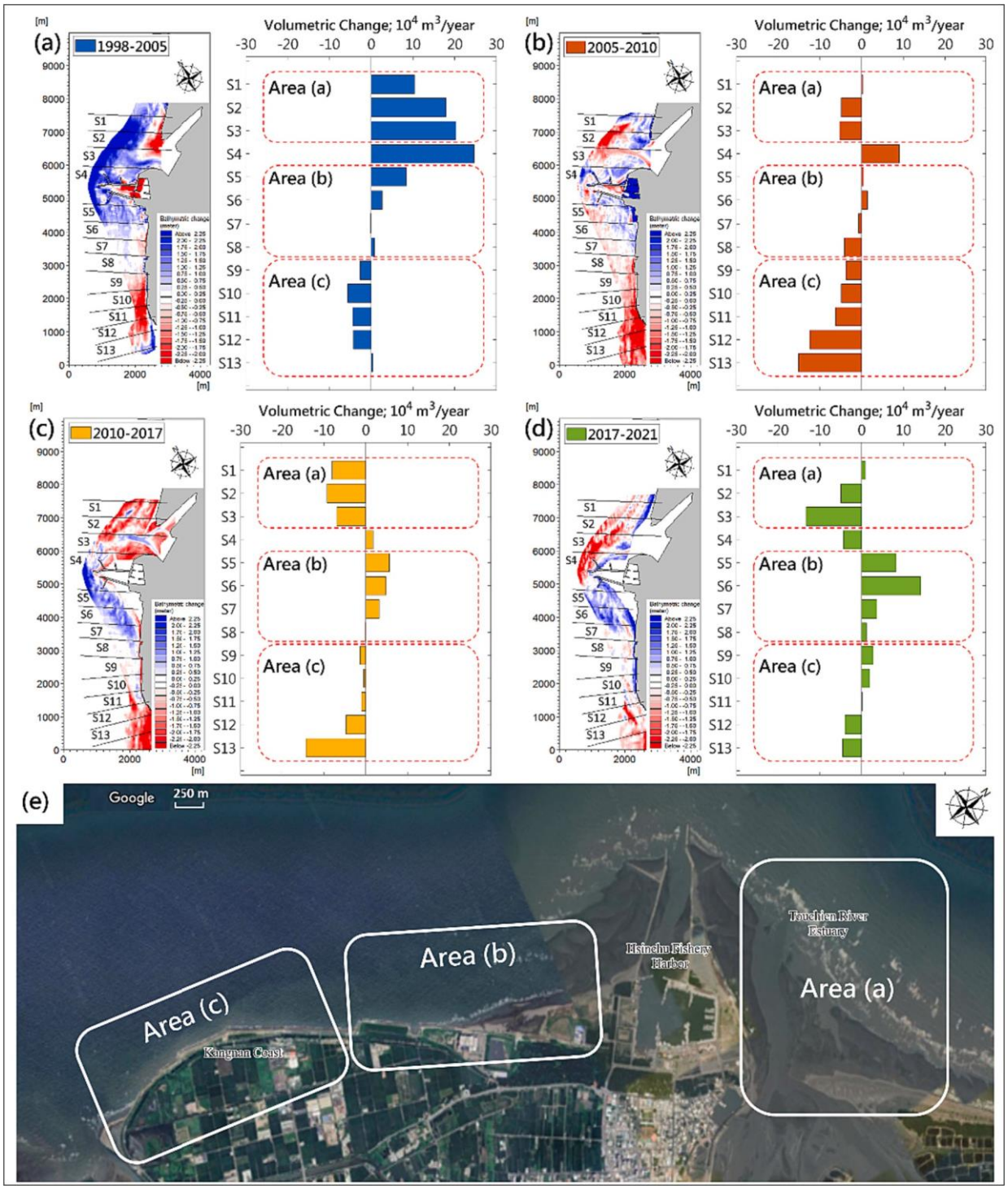

Fig. 5. Bathymetric changes of Hsinchu coast: (a) 1998 to 2005; (b) 2005 to 2010; (c) 2010 to 2017; and (d) 2017 to 2021. Blue color indicates accretion, while red color indicates erosion. Each bar chart shows the accretion (positive values) and erosion (negative values) rates for each section during the periods 1998–2005 (blue bar), 2005–2010 (orange bar), 2010–2017 (yellow bar), and 2017–2021 (green bar). According to the spatial characteristics, (e) shows the division of the coast into three sections: Area (a), S1–S3; Area (b), S5–S8; and Area (c), S9–S13. (For interpretation of the references to color in this figure legend, the reader is referred to the web version of this article.)

2010 and 2017, and Fig. 5d shows the bathymetric changes between 2017 and 2021. The blue color in the image represents positive values, indicating accretion, while the red color represents negative values, indicating erosion. The rates of accretion and erosion were calculated for each section during the different time periods to determine whether the sediment volume along the Hsinchu Coast was increasing or decreasing (Fig. 5a–d, histograms).

According to the results, the temporal variation of coastal morphological changes can be divided into three intervals: Period 1 (1998 to 2005, P1) is characterized by accretion in Touchien River Estuary and both sides of Hsinchu Fishery Harbor, as well as erosion on the south side of Hsinchu Fishery Harbor, from Kangnan seawall to Kerya river. In Period 2 (2005 to 2010, P2), the estuary started to erode and the range from Kangnan seawall to Kerya river was still eroding. Then, in Period 3

(2010 to 2017 and 2017 to 2021, P3), erosion can be observed throughout the coast, except for the sheltered area on the south side of Hsinchu Fishery Harbor. According to the bathymetric change analysis, this study divided the research area into three subareas. Areas (a), (b), and (c) represent the estuary region (S1–S3), sheltered zone (S5–S8), and the region from Kangnan coast to Kerya river (S9–S13), respectively. The net changes in bathymetric volume around Hsinchu coast are presented in Fig. 5. The change of bathymetric volume in Area (a) indicated a net accretion of 3.4×10^6 m^3 with an average accretion rate of 4.9×10^5 m^3/year from 1998 to 2005, as shown in Fig. 5a. However, from 2005 to 2010, 2010 to 2017, and 2017 to 2021, area (a) experienced net erosion of $-4.9\ 10^5$ m^3, $1.7\ -10^6$ m^3, and $6.9\ 10^5$ m^3, respectively, with corresponding average erosion rates of $9.8\ 10^4$ m^3/year, $\times\ 2.4\ 10^5$ m^3/year, and $1.7\ \ 10^5$ m^3/year, as shown in Fig. 5b, c, d. To the contrary, the volumetric change results for area (b) indicated that the sheltered zone (S5–S8) experienced net accretion of 8.2×10^5 m^3, 9.5×10^5 m^3, and 1.1×10^6 m^3 during the time periods of 1998 to 2005, 2010 to 2017, and 2017 to 2021, respectively, with corresponding average accretion rates of $1.2\ 10^5$ m^3/year, 1.4×10^5 m^3/year, and 2.7×10^5 m^3/yr. However, during the time period from 2005 to 2010, the sheltered zone experienced net erosion of $-\ 1.5 \times 10^5$ m^3, with an average erosion rate of $-\ 2.9 \times 10^4$ m^3/yr. Fig. 5 also depicts the volumetric changes in area (c), revealing that the region from Kangnan coast to Kerya river (S9–S13) experienced a consistent net erosion with total amounts of -1.2×10^5 m^3, -2.1×10^6 m^3, -1.5×10^6 m^3, and -1.4×10^5 m^3 over the four time periods, with corresponding average erosion rates of -1.6×10^5 m^3/year, -4.2×10^5 m^3/year, -2.2×10^5 m^3/year, and -3.6×10^4 m^3/year, respectively.

During P1 (Fig. 5a), the morphological changes along the Hsinchu coast were significantly affected by Hsinchu Fishery Harbor, altering the original hydrodynamic mechanism and obstructing littoral sediment transport. Therefore, the bathymetric changes from 1998 to 2005 presented a severe disequilibrium in erosion and accretion from the north to the south of the harbor. This means that, as Hsinchu Fishery Harbor blocks littoral sediment transport, sediments must be accumulated to a certain extent in the north end of the harbor before they can bypass the groin to the south side of the harbor. When the sediments come to the sheltered area, the sediment begins to accrete in S5–S8 due to the significant reduction in wave energy, leading the sediments to not pass to S9–S13. Moreover, in the southern region of the coast (S9–S13), the original wave energy returns, and less sediment is accreted, causing erosion to become more serious. In contrast, during P2 (Fig. 5b), the shelter zone and estuary started to erode, especially in the waterway, due to an insufficient supply of fluvial sediment caused by decreased river discharge from 2005 to 2010 compared to 1998 to 2005. Additionally, comparing Fig. 5b to Fig. 5a, areas (a) and (b)—namely, the estuary and shelter zone—shifted from accretion to erosion. Further south, in area (c), the erosion became more severe along the coast from S9 to S13. The observed morphological changes in this time period provide an obvious sign that the river flow magnitude directly affects the morphological changes of the Hsinchu Coast, especially that in Touchien River Estuary. In P3 (Fig. 5c, d), similar morphological characteristics were observed for Hsinchu coast during the time period of 2010 to 2017 and 2017 to 2021. The estuary continued to erode due to the decreased river discharge from 2010 to 2021, compared to 1998 to 2010. Although the erosion in the estuary was more serious than in the past two periods, the sheltered area began to present obvious accretion, and the extent of erosion in Kangnan area also slowed down. The morphological pattern in P3 proves that the Hsinchu coast has presented a new morphological dynamic equilibrium over the past decade, instead of the previous groin effect.

3.3. *Principal mode of coastal morphological changes and corresponding weighting*

EOF analysis was performed on a bathymetric survey data set of the Hsinchu coast in order to explore the major and minor modes of its long-term evolution. This study divided the EOF analysis into two distinct time periods; namely, 2005 to 2010 (with low wave energy and high river discharge) and 2017 to 2021 (with high wave energy and low river discharge). Nine bathymetric survey data sets covering the period between 1998 and 2021 were interpolated and transformed into two regular grids with dimensions of 1800 m × 1000 m and 1400 m × 4200 m. These grids consisted of a total of 19,200 elements and are illustrated in Fig. 6. The bathymetric change analysis areas (a), (b), and (c) were also included in the EOF method analysis. This approach facilitated a comparison of the EOF analysis results with the results of the bathymetric change analysis, which provided more information from the data set. The procedure successfully separated the data set into several independent modes, each with spatial eigenfunctions (spatial components) and temporal coefficients (temporal components). Spatial values indicated the impact ranges of the corresponding impact factors, while the temporal coefficients described the annual variation of the impact factors.

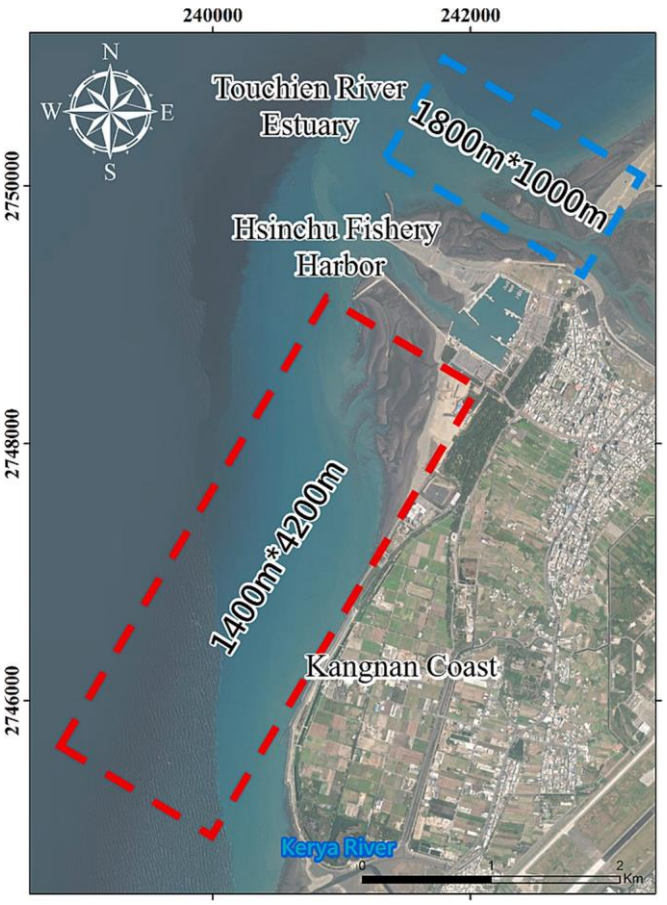

Fig. 6. EOF analysis area. The blue rectangle shows a 1800 m × 1000 m grid comprising 14,700 elements, while the red rectangle shows a 1400 m × 4200 m grid comprising 4500 elements. (For interpretation of the references to color in this figure legend, the reader is referred to the web version of this article.)

The EOF analysis results, based on the two time periods, included the first two spatial eigenfunctions of the model and the corresponding temporal coefficients, as represented in Fig. 7. As the first two modes of the EOF analysis results explained most of the variability, it was not considered necessary to integrate the remaining modes into the analysis; in particular, the EOF analysis results indicated that the two possible modes accounted for more than 98% of the variability observed on Hsinchu coast, as detailed in Table 1. The first mode in the EOF results revealed the most significant morphological changes, accounting for 93.61% (2005–2010) and 98.29% (2017–2021) of the co-variability in

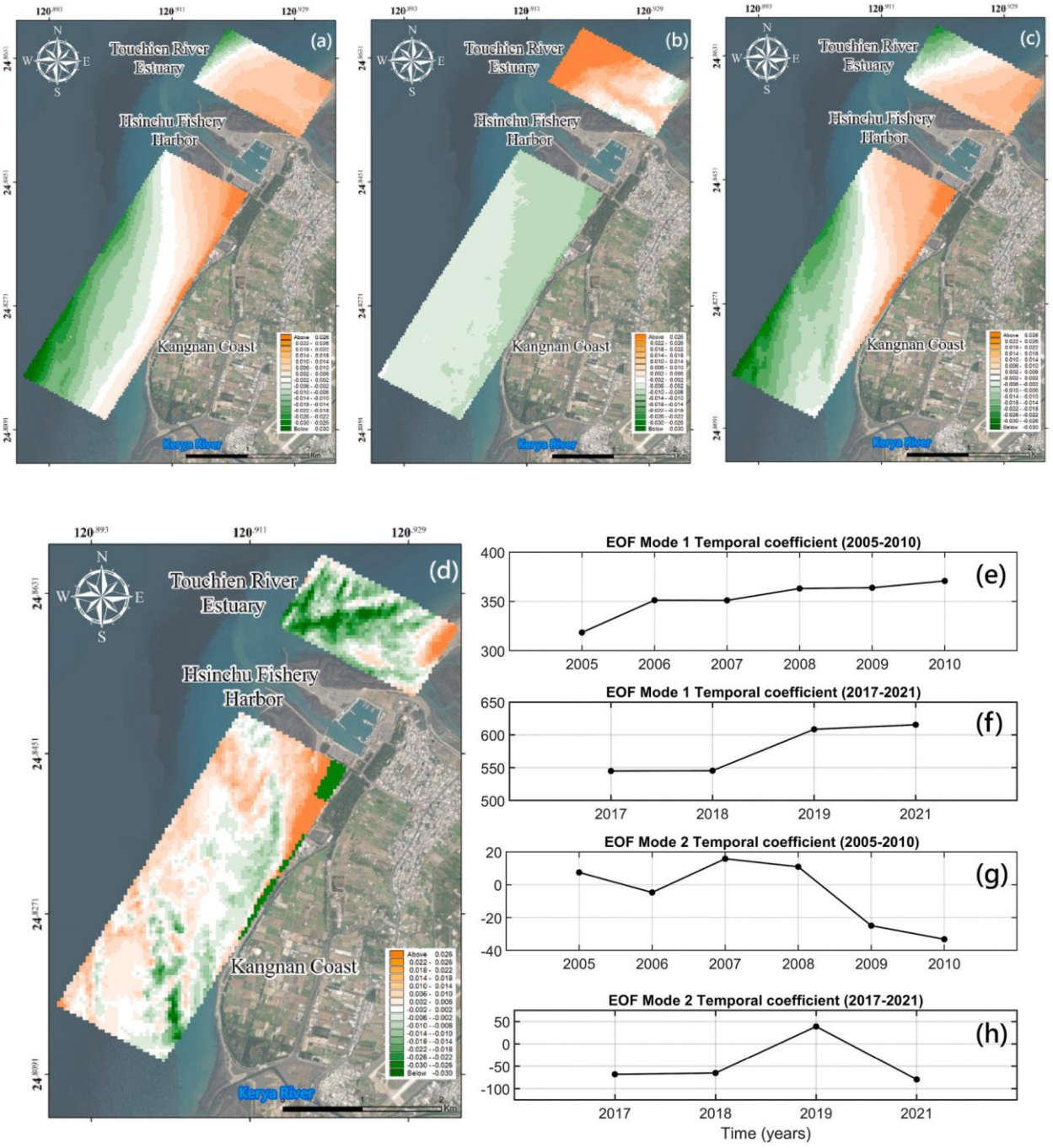

Fig. 7. Plots of the spatial eigenfunctions (spatial components) and the corresponding temporal coefficients (temporal components) of the first two main components of morphological variability in Hsinchu coast. The color represents the amplitude of the corresponding spatial eigenfunctions (m): (a) First spatial eigenfunctions and (e) corresponding temporal coefficients from 2005 to 2010; (b) second spatial eigenfunctions and (f) corresponding temporal coefficients from 2005 to 2010; (c) first spatial eigenfunctions and (g) corresponding temporal coefficients during 2017 to 2021; and (d) second spatial eigenfunctions and (h) corresponding temporal coefficients during 2017 to 2021.

Table 1
Percentage of variability in the first two modes obtained in the EOF analysis.

	Mode-1	Mode-2	Total of EOF-Mode1 and EOF-Mode2	Remain
2005–2010	93.61%	5.21%	98.82%	1.18%
2017–2021	98.29%	1.22%	99.51%	0.49%

elevation. Therefore, spatial characterization of the first mode revealed the influence of the interaction of waves and structures on the change in coastal morphology (Fig. 7a, c). On the two sides of Hsinchu Fishery Harbor, the positive components in the updrift area were due to the structures blocking the littoral sediment transport, thus forming a deposition area, while the positive components in the downdrift were caused by the interaction between structures and waves, forming a sheltered area and causing sediment deposition in this region. The corresponding temporal coefficients for the first mode in the two time periods indicated an increasing coefficient, ranging from 318.4 to 370.75

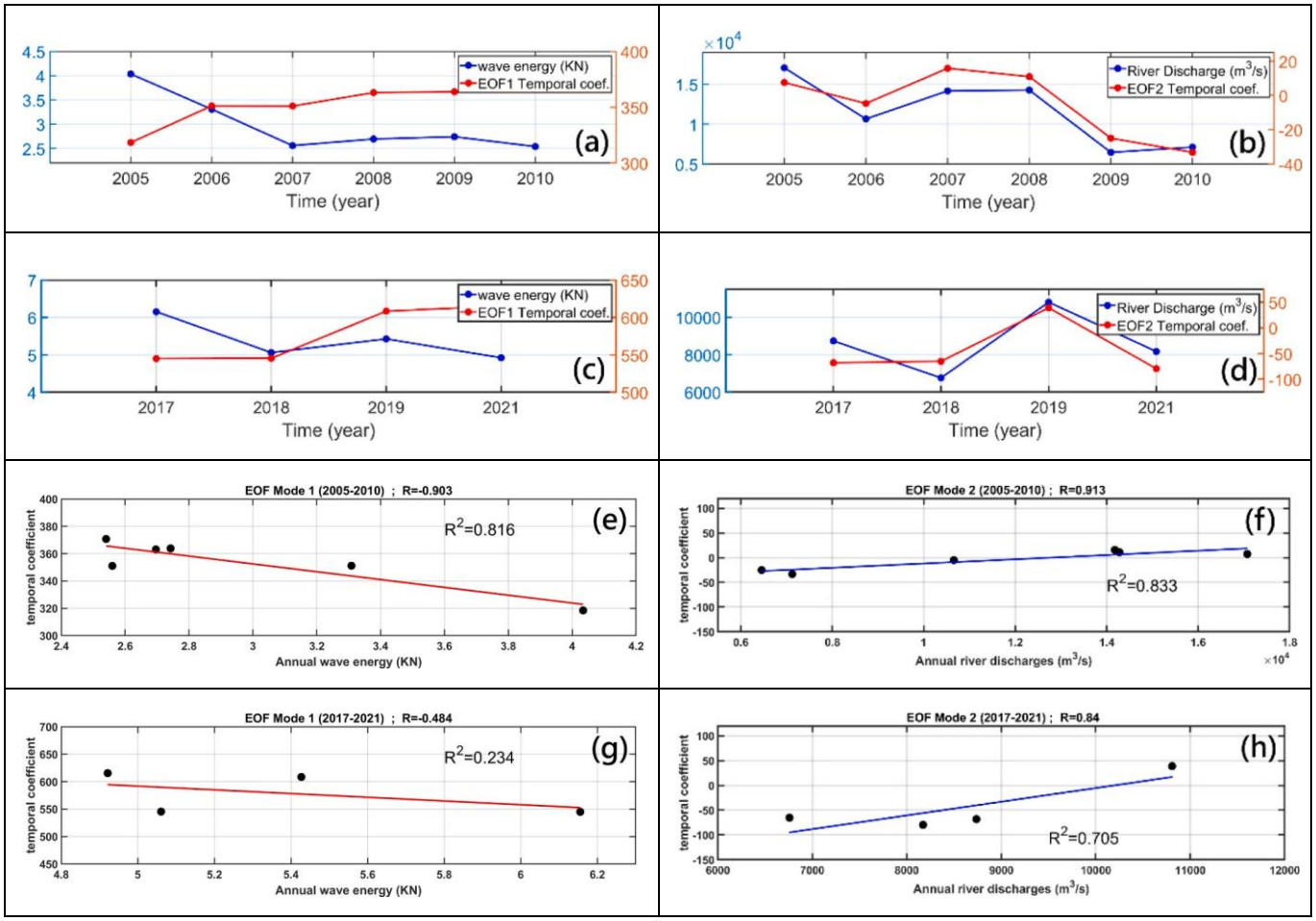

Fig. 8. Comparison of temporal coefficients of the first mode and annual wave energy: (a) In the time period from 2005 to 2010; and (c) in the time period from 2017 to 2021. Comparison of temporal coefficients of the second mode and river discharges: (b) In the time period from 2005 to 2010; and (d) in the time period from 2017 to 2021. Relationship between the temporal coefficients of the first mode and annual wave energy at Hsinchu coast with the red fitting line: (e) In the time period from 2005 to 2010; and (g) in the time period from 2017 to 2021. Temporal coefficients of the second mode and annual discharges at Touchien River Estuary with the blue fitting line: (f) In the time period from 2005 to 2010; and (h) in the time period from 2017 to 2021. (For interpretation of the references to color in this figure legend, the reader is referred to the web version of this article.)

in 2005–2010 (Fig. 7e) and 544.91–615.46 in 2017–2021 (Fig. 7f). Although the EOF temporal coefficients of the first mode in the two time periods were inversely proportional to the yearly variation of wave energy (Fig. 8a, c), the temporal pattern of the annual wave energy and corresponding temporal coefficients from 2005 to 2010 showed a very statistically similar pattern (R^2 = 0.81; Fig. 8 g). Therefore, it can be inferred that the positive components (orange color) represent the morphological changes related to the structure, while the negative components (green color) represent those not related to the structure.

Table 2
Average River discharges (m^3/year) and average wave energy (KN) were calculated for different time intervals.

	Calculated Period	Interval (Year)	Average River Discharge (m^3/Year)			Average Wave Energy (KN)
			TCR	FSR	Total	
1	1998 2005	7	8916.74	3410.29	12,327.03	4.10
2	2005 2010	5	7542.50	4041.53	11,584.03	2.98
3	2010 2017	7	6583.67	3953.42	10,537.09	5.08
4	2017 2019	2	6201.71	2565.91	8767.62	5.55
5	2019 2021	2	5901.23	1596.07	7497.30	4.96

The second mode of the EOF analysis results explained 5.21% (2005–2010) and 1.22% (2017–2021) of the co-variability in elevation. The spatial components of the second mode reflected the influence of the interaction of river discharges and structures on the change of coastal morphology (Fig. 7c, d). In Fig. 7c, the positive components in updrift indicate an obvious water path where the water depth exceeds 0 m. Notably, the component width of Touchien River's water path is wider than that of Fengshan River; this reflects the actual physical phenomenon in Touchien River, whose discharges from 2005 to 2010 were generally greater than those of Fengshan River. When the water depth is below 0 m, the positive components clearly show signs of river discharge affecting coastal morphological change. As a result of the large reduction in river discharge, the original positive component in the upper reaches of Fig. 7c was replaced with a negative component in Fig. 7d.

The corresponding temporal coefficients of the second mode in the two time periods showed the coefficient ranging from —33.21 to 15.80 in 2005–2010 (Fig. 7g) and — 79.55 to 38.86 in 2017–2021 (Fig. 7h). There was a very strong correlation between the temporal coefficients and corresponding river discharges (Fig. 8b, d). Moreover, comparing the statistical relationship between temporal coefficients and corresponding river discharges, it was found that the results represented very high correlations (R^2 = 0.833 and R^2 = 0.705; Fig. 8f, h). The findings

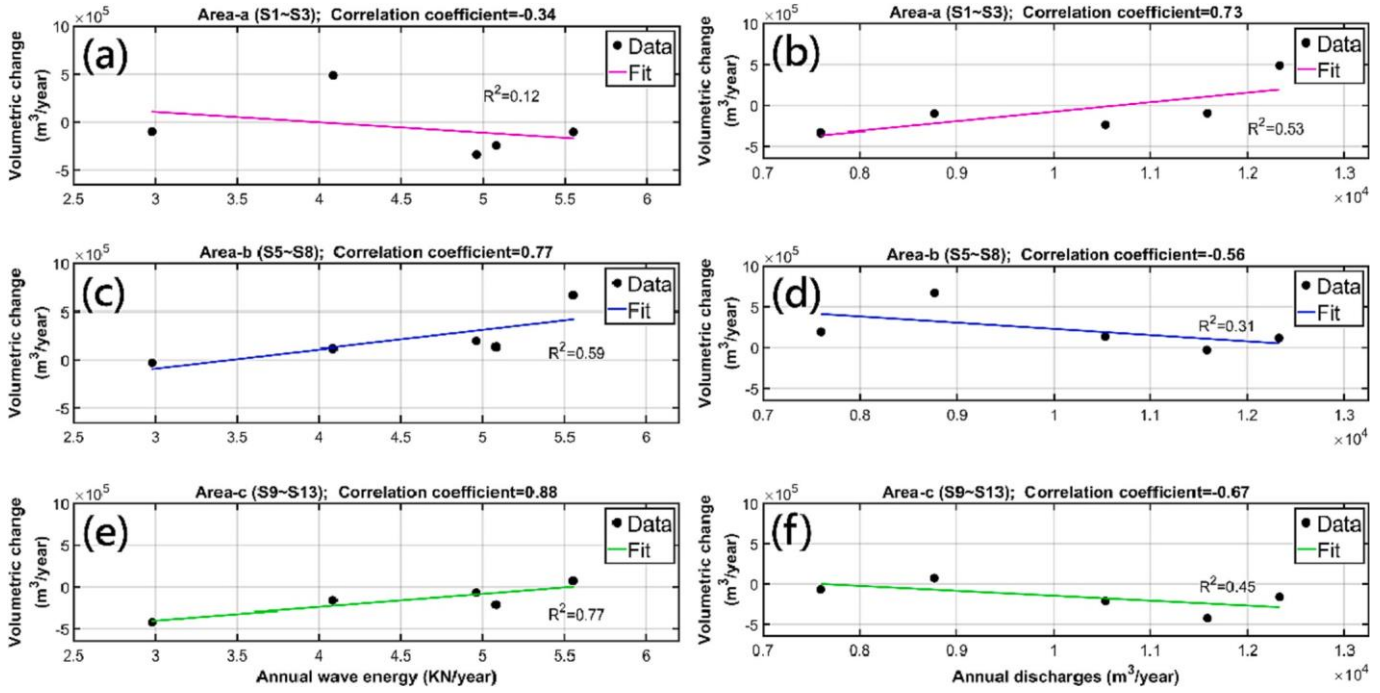

Fig. 9. Relationship between the volumetric change in Areas (a), (b), and (c) and average wave energy at Hsinchu coast (a, c, e); and the relationship between the volumetric change in Areas (a), (b), and (c) and average discharge from Touchien River estuary (b, d, f).

indicate that, akin to the first mode, the positive components of the second mode depict the morphological variations linked to river discharge, whereas the negative components depict those not associated with river discharge.

4. Discussions

4.1. Possible relationship between impact factors and different regions

Wave forcing and river discharge are important factors that significantly influence the morphological changes in the vicinity of Hsinchu Fishery Harbor. This study endeavored to examine the connection between coastal morphological alterations and natural factors, such as wave forcing and river discharge, and to establish a correlation between them. Correlation coefficients (R) were calculated to estimate the degree of correlation between annual wave energy, river discharge, and bathymetric changes. Table 2 presents the average river discharges and wave energy during different time intervals from 1998 to 2021, which were obtained from annual hydrological reports and wave buoy records. The mean river discharges during the 7-year period of 1998–2005, the 4-year period of 2005–2010, the 7-year period of 2010–2017, the 3-year period of 2010–2017, and the 3-year period of 2019–2021 were 12,327.03 m^3/s, 11,584.03 m^3/s, 10,507.09 m^3/s, 8767.62 m^3/s, and 7497.30 m^3/s, respectively. The average wave energies during the same time intervals were 4.10 KN/m, 2.98 KN/m, 5.08 KN/m, 5.55 KN/m, and 4.96 KN/m, respectively. Fig. 9 illustrates the correlations between river discharges, wave energy, and the bathymetric volume for each area.

The findings shown in Fig. 9 indicate that there exists a significant relationship between temporal bathymetric changes and natural factors such as river discharge and wave energy. Specifically, Fig. 9b demonstrates a correlation (R = 0.73) between the bathymetric changes in Touchien River estuary (S1–S3, Are a) and average river discharge. Meanwhile, Fig. 9c demonstrates that there was a strong correlation (R = 0.88) between the bathymetric changes in the shelter area (S5–S8; Area b) and wave energy. Fig. 9e demonstrates that there was a strong correlation (R = 0.88) between the bathymetric changes in Kangnan coast (S9–S13; Area c) and wave energy. Moreover, comparing the net bathymetric volume changes with average river discharge, it was observed that river discharge did not significantly affect the coast south of the harbor, but did impact the morphology of the coast north of the harbor (Fig. 9b, d, and f). Meanwhile, comparing the net bathymetric volume changes with wave energy, it was observed that wave energy did not significantly affect the coast north of the harbor, but did impact the morphology of the coast south of the harbor (Fig. 9a, c, and e). According to the above, the statistical results reveal that the volumetric changes in Touchien estuary (S1–S3, Area a) were mainly affected by river discharge (Fig. 9a, b). Similarly, the volumetric changes in Kangnan coast (S9–S13, Area c) were mainly affected by wave forcing (Fig. 9e, f). However, these results do not imply that the coastal morphological changes in each region are solely influenced by one particular factor. The volumetric changes in the shelter area (S5–S8, Area b) presented dissimilarities in both wave energy and river discharge, implying that the coastal morphology in this region is complex and influenced by various factors (Fig. 9c, d). Specifically, the coastal bathymetric changes in Hsinchu coast were affected by both river flow and wave energy, but in different weights and different positions.

4.2. Anthropogenic influences at Hsinchu coast

The presence of structures within the study area was a constant variable. Thus, the impact of structures on coastal morphological changes was considered dependent on the combined effects of structures and other influencing factors. Analysis of the EOF results from 2005 to 2010 and 2017 to 2021 demonstrated that the weights of the first mode, which represents the interaction between wave energy and structures in coastal morphological changes, were 93.61% and 98.29%, respectively. Despite the significant increase in wave energy (from 2.98 KN to 5.22 KN) between the two time periods—with a rate of increase of 75.2%—the corresponding weighting only changed slightly (by 4.68%). The second mode in the EOF analysis represented the interaction between river discharge and structures in coastal morphological changes, with corresponding weightings of 5.21% and 1.22% for the two time periods,

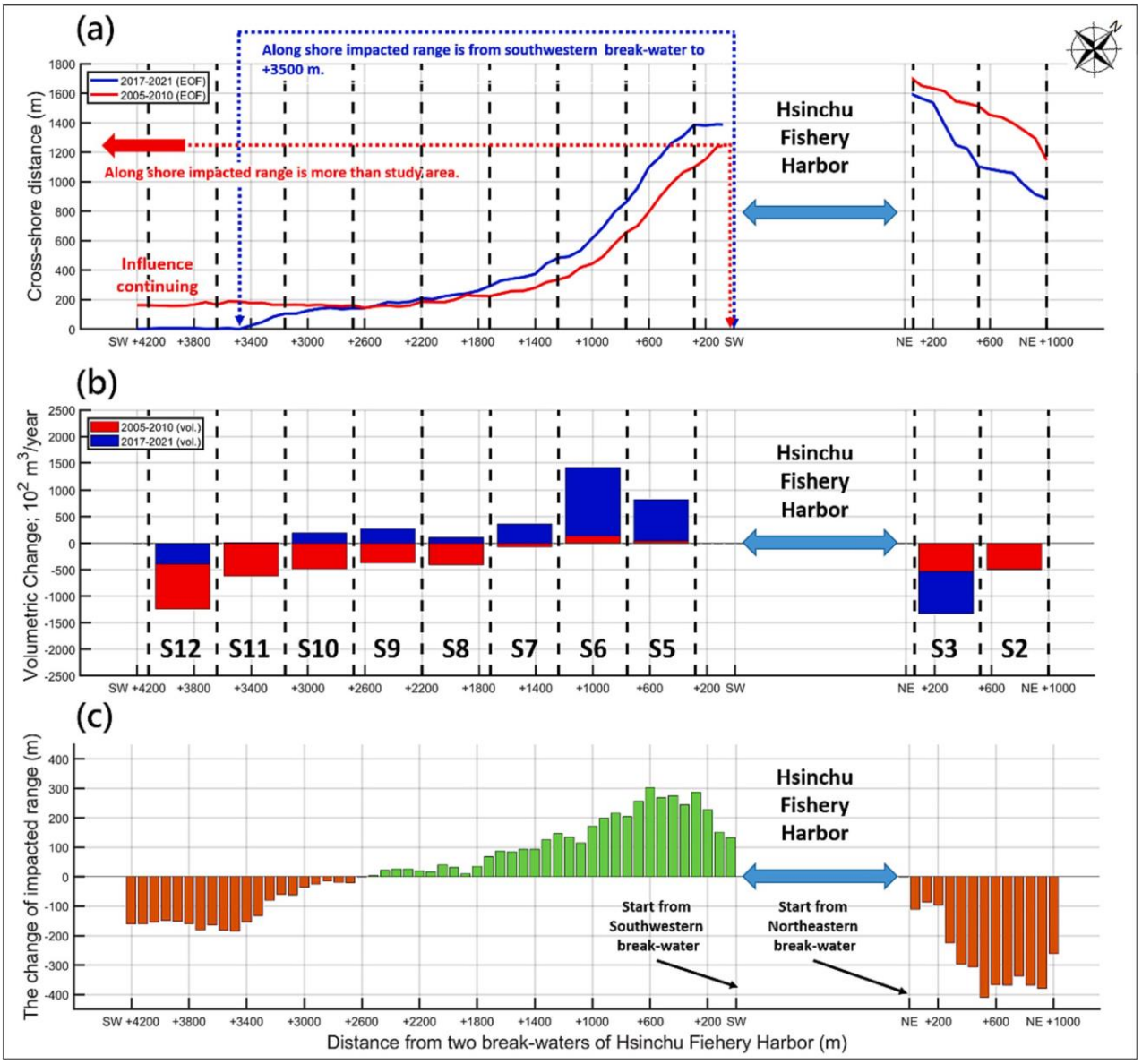

Fig. 10. (a) 1D impact range regarding the first mode in the EOF analysis. The red and blue lines represent the analysis results in the time periods 2005–2010 and 2017–2021, respectively; (b) bathymetric changes of Hsinchu coast during the time periods 2005–2010 (blue bars) and 2017–2021(red bars); and (c) the change in the cross-shore impact range between the two periods (2017–2021 and 2005–2010), where the green bars indicate an increase and the orange bars indicate a decrease. (For interpretation of the references to color in this figure legend, the reader is referred to the web version of this article.)

respectively, resulting in a change of only 3.99%. However, the average river discharge showed a 24.3% downward trend over the two time periods, decreasing from 11,584.03 m^3/year to 8767.62 m3/year. These findings highlight the complex nature of the relationship between the measured value and weighting value of each impact factor in the study area. Specifically, although the change in influence weights do not demonstrate proportional variations in response to changes in wave energy and river discharge magnitudes, the results still indicated that the interactions between wave energy and structures is still the primary impact factor affecting the study area.

To determine the impact range resulting from anthropogenic effects—namely, the interaction between wave energy and structures—the cross-shore and alongshore impact ranges were obtained from the boundary between the positive and negative spatial components of the first two modes in Fig. 7a and c as illustrated in Fig. 10a. The changes of the cross-shore impact range between the two periods are presented in Fig. 10c. Furthermore, the bathymetric changes for the two time periods were compared to Fig. 10b, in order to verify the reasonableness of the determined impact range. As shown in Fig. 10a and c, between 2005 and 2010, the impact range along the south-west side of the harbor had a trend that should continue to extend further to the southwest (red color), but the analysis results cannot be displayed due to insufficient bathymetric survey data on this side. Meanwhile, the impact range along the coast only reached SW+3500 between 2017 and 2021 (blue color). The cross-shore impact range showed a clear tendency to extend offshore in the SW+0 to SW+1800 range, with a maximum change of 303.01 m, while it retreated to the land side in the SW-3100 to SW+4200 range, with a maximum change of −185.99 m. In the SW-1800 to SW+3100 range, the change in the impact range was less than 50 m, indicating that the interaction between structures and wave energy did not directly or indirectly alter the cross-shore impact range in this area. In NE+200 to NE+1000 range, between 2005 and 2010, wave energy was relatively low, so most of the sediment was deposited in the estuary. However, during 2017–2021 (blue), the wave energy was higher than 2005–2010,

bringing the original sediment in the estuary to the south of the fishing port, thus affecting the area the impact range on the northeast side of the harbor retreated to the land side with a maximum change of 408.01 m (Fig. 10a, c). Therefore, considering the increase in average wave energy from 2.98 KN to 5.22 KN and the changes in the influence range for the two time periods, it can be inferred that the power of the wave energy is the primary cause of the impact range. Comparing the impact range obtained through the EOF analysis with the results of historical volumetric changes from 2005 to 2010 and 2017–2021 (Fig. 10b), the S11 interval was found to be a critical turning point at the moment of morphological change from erosion to accretion, and also defines the impact range of structures, which is affected by the interaction between structures and wave energy. Based on historical data and the EOF results, the minimum impact range of structures was 3.5 km south of Hsinchu Fishing Harbor.

5. Conclusions

Through the collection of basic data and analysis of historical morphological changes, it was found that the morphological changes in Hsinchu coast were affected by the groin effect of the breakwater of the Hsinchu Fishing Harbor, which disrupted the continuity of sediment transport from the north to the south or sediment transport from the river mouth to the ocean. As a result, significant erosion occurred on the south side and accretion on the north side of the harbor from 1998 to 2005. However, after 2005, the coastal morphological changes were no longer characterized by erosion on the north of the harbor and accretion on the south of the harbor, and were influenced by the magnitude of wave energy and river discharge. To further understand the interaction between river flow and structures, as well as the interaction between wave energy and structures, in relation to their degree of influence on coastal morphological changes, this study analyzed coastal morphological changes during two periods affected by different scenarios (2005 to 2010, with lower wave energy and higher river discharges, and 2017 to 2021, with higher wave energy and lower river discharges) and utilized the EOF analysis method to determine the primary and secondary influencing factors. According to the EOF analysis results, the main factor affecting coastal morphological changes over the past 20 years was the interaction between wave energy and the structures, while the interaction between river discharge and structures was the secondary factor. Furthermore, through a comparison of the spatial distribution obtained in the EOF analysis and the historical morphological change analysis results, it was inferred that the minimum impact range of the structures on coastal morphological interaction changes was 3.5 km south of the Hsinchu Fishing Harbor. In summary, the appearance of structures will inevitably lead to irreversible impacts on and changes to the coastal morphology, becoming the main influencing factor affecting coastal morphological changes. However, over time, coastal morphological changes will gradually reach a new dynamic equilibrium, and the main factors influencing coastal morphological changes will shift from structures to natural factors. This study provides insights into the morphological changes induced by anthropogenic structures and their combined impacts with natural processes, and it can inform the development of effective coastal management strategies.

Declaration of Competing Interest

The authors declare that they have no known competing financial interests or personal relationships that could have appeared to influence the work reported in this paper.

Data availability

Data will be made available on request.

Acknowledgments

This work was partly supported by the Ministry of Science and Technology, Taiwan, Project no. MOST111-2625-M-019-003-. Their support is deeply appreciated.

References

Alvare, F., Pan, S.Q., 2016. Predicting coastal morphological changes with empirical orthogonal function method. Water Sci. Eng. 9, 14–20.
Boak, E.H., Turner, I.L., 2005. Shoreline definition and detection: a review. J. Coast. Res. 21, 688–703.
Boyd, R., Dalrymple, R.W., Zaitlin, B.A., 1992. Classification of clastic coastal depositional environments. Sediment. Geol. 80, 139–150.
Buonaiuto, F.S., Bokuniewicz, H.J., FitzGerald, D.M., 2008. Principal component analysis of morphology change at a tidal inlet: Shinnecock inlet, New York. J. Coast. Res. 24, 867–875.
Chang, H.H., 1997. Modeling fluvial processes in tidal inlet. J. Hydraul. Eng. 123, 1161–1165.
Construction and Planning Agency of the Ministry of the Interior (CPAMI), 2017. Integrated Coastal Zone Management Plan. From. https://www.cpami.gov.tw/filesys/file/chinese/dept/rp3/rp1060206.pdf.
Dalrymple, R.W., Mackay, D.A., Ichaso, A.A., Choi, K.S., 2012. Processes, morphodynamics, and facies of tide-dominated estuaries. In: Davis Jr., R.A., Dalrymple, R.W. (Eds.), Principles of Tidal Sedimentology. Chap. 5. Springer, Dordrecht, pp. 79–107, 2012.
Dean, R.G., 1986. Sediment budget principles and applications. In: Proceedings of the Dynamics of Sand Beaches, International Conference on Coastal Engineering (ICCE) 20th Taipei, Taipei, Taiwan, 29 January.
Delgadillo-Calzadilla, M.A., Mendoza, E., Silva, R., González-Vázquez, J.A., Infante-Mata, D., 2014. Beach erosion in San Benito Chiapas, Mexico: assessment and possible solution. J. Coast. Res. 71, 131–136.
Ding, Y., Wang, S.S.Y., 2008. Development and application of a coastal and estuarine morphological process modeling system. J. Coast. Res. 52, 127–140.
Fredsøe, J., Deigaard, R., 1992. Mechanics of coastal sediment transport. In: Advanced Series on Ocean Engineering, 3,1st ed. World Scientific, Singapore, pp. 1–369.
Gopinath, G., Seralathan, P., 2005. Rapid erosion of the coast of Sagar island, West Bengal – India. Environ. Geol. 48, 1058–1067.
Habel, S., Fletcher, C.H., Barbee, M., Anderson, T.R., 2016. The influence of seasonal patterns on a beach nourishment project in a complex reef environment. Coast. Eng. 116, 67–76.
Hallermeier, R.J., 1981. A profile zonation for seasonal sand beaches from wave climate. Coast. Eng. 4, 253–277.
Harley, M.D., Turner, I.L., Short, A.D., Ranasinghe, R., 2015. Extreme coastal erosion enhanced by anomalous extratropical storm wave direction. Nat. Geosci. 8, 681–686.
He, Y., Wu, Y., Lu, C., Wu, M., Chen, Y., Yang, Y., 2019. Morphological change of the mouth bar in relation to natural and anthropogenic interferences. Cont. Shelf Res. 175, 42–52.
Holden, W.N., Marshall, S.J., 2018. Climate change and typhoons in the Philippines: extreme weather events in the Anthropocene. Integr. Disaster Sci. Manag. 407–421.
Hsu, T.W., Lin, T.Y., Tseng, I.F., 2017. Human impact on coastal erosion in Taiwan. J. Coast. Res. 23, 961–973.
Hsu, J.C., Huang, W.P., Lin, J.G., 2018. The influence of coastal developments on the coastal changes at Hsinchu coast, Taiwan. In: Proceedings of the 28th International Ocean and Polar Engineering Conference, Sapporo, Japan, 10–15 June.
Hu, Y., Cao, M., Ma, A., Dou, X., Wen, Y., 2020. An analysis of the periodic evolution of the Jingjiang sandbank in the tidal reach of the Yangtze River. Water 12, 1652.
Huang, W.P., 2022. Impact of coastal development on coastal morphology of Taiwan: case studies and proposed countermeasures. J. Sea Res. 186, 102234.
Karunarathna, H., Reeve, D., Spivack, M., 2008. Long-term morphodynamic evolution of estuaries: an inverse problem. Estuar. Coast. Shelf Sci. 77, 385–395.
Keshtpoor, M., Puleo, J.A., Gebert, J., Plant, N.G., 2013. Beach response to a fixed sand bypassing system. Coast. Eng. 73, 28–42.
Kim, I.H., Lee, H.S., Cho, W.C., Song, D.S., 2013. Shoreline changes due to groin construction in Namae and Sodol beaches, South Korea. J. Coast. Res. 65, 2131–2136.
Komar, P.D., 1999. Coastal change-scales of processes and dimensions of problems. In: Coastal Sediments '99: Proceedings of the 4th International Symposium on Coastal Engineering and Science of Coastal Sediment Processes, Civil Eng, pp. 1–17.
Liou, J.C., Chang, H.K., Liaw, S.R., 2009. Beach Erosion and preventive countermeasure at Kangnan coast, Taiwan. J. Coast. Res. 25, 405–416.
Martins, K.A., Pereira, P.S., 2014. Coastal erosion at Pau Amarelo Beach, northeast of Brazil. J. Coast. Res. 71, 17–23.
Masselink, G., Scott, T., Poate, T., Russell, P., Davidson, M., Conley, D., Sutherland, J., 2016. Extreme wave activity during 2013/2014 winter and morphological impacts along the Atlantic coast of Europe. Geophys. Res. Lett. 43, 5039–5048.
Mentaschi, L., Vousdoukas, M.I., Pekel, J.F., Voukouvalas, E., Feyen, L., 2018. Global long-term observations of coastal erosion and accretion. Sci. Rep. 8, 12876.
Miller, J.K., Dean, R.G., 2007a. Shoreline variability via empirical orthogonal function analysis: part I temporal and spatial characteristics. Coast. Eng. 54, 111–131.
Miller, J.K., Dean, R.G., 2007b. Shoreline variability via empirical orthogonal function analysis: part II temporal and spatial characteristics. Coast. Eng. 54, 133–150.
Nicholls, R.J., Hanson, S., Herweijer, C., Patmore, N., Hallegatte, S., Corfee-Morlot, J., Château, J., Muir-Wood, R., 2007. Ranking Port Cities with High Exposure and

Vulnerability to Climate Extremes—Exposure Estimates, OECD Environmental Working Paper. OECD, Paris, Franch, pp. 1–51.
Nishi, R., 2008. The mechanism of debris transport from inland to nearshore zone. Bull. Coast. Oceanogr. 2008 (45), 97–103.
Reeve, D.E., Horrillo-Caraballo, J.M., Magar, V., 2018. Statistical analysis and forecasts of long-term sandbank evolution at Great Yarmouth, UK. Estuar. Coast. Shelf Sci. 79, 387–399.
Rosati, J.D., 2005. Concepts in sediment budgets. J. Coast. Res. 21, 307–322.
Sumer, B.M., Sumer, S., Whitehouse, R.J.S., 2001. Scour around coastal structures: a summary of recent research. Coast. Eng. 42, 67–93.
Taaouati, M., Parisi, P., Passoni, G., Lopez-Garcia, P., Romero-Cozar, J., Anfuso, G., Vidal, J., Munoz-Perez, J.J., 2020. Influence of a reef flat on beach profiles along the Atlantic coast of Morocco. Water 12 (3), 790.
Tanaka, H., Viet, N.T., Hoang, V.C., Duy, D.V., 2015. Erosion mechanism on Cua Dai Beach, Central Vietnam. J. Jpn. Soc. Civ. Eng. 71, I449–I454 (In Japanese).
Thanh, T.M., Tanaka, H., Mitobe, Y., Viet, N.T., Almar, R., 2018. Seasonal variation of morphology and sediment movement on Nha Trang coast, Vietnam. J. Coast. Res. 81, 22–31.
van Rijn, L.C., 2011. Coastal erosion and control. Ocean Coast. Manag. 54, 867–887.
Winant, C.D., Inman, D.L., Nordstrom, C.E., 1975. Description of seasonal beach changes using empirical eigenfunctions. J. Geophys. Res. 80, 1979–1986.
Yuhi, M., Dang, M.H., Umeda, S., 2013. Comparison of accelerated erosion in riverbed and downstream coast by EOF analysis. J. Coast. Res. 65, 130–135.